UDC 551.515.21:551.511.6:551.513.1

THE ROLE OF LARGE-SCALE ASYMMETRIES AND INTERNAL MIXING IN COMPUTING MERIDIONAL CIRCULATIONS ASSOCIATED WITH THE STEADY-STATE HURRICANE

RICHARD A. ANTHES

National Hurricane Research Laboratory, ESSA, Miami, Fla.

ABSTRACT

The role of asymmetries (large-scale horizontal eddies) in satisfying the mean angular momentum budget for the steady-state hurricane is studied by computing transverse circulations for a prescribed tangential vortex on the scale of 1000 km. For realistic diabatic heating rates at large distances from the hurricane center, the correlation between radial velocity and absolute vorticity must be negative in the upper troposphere and positive in the lower troposphere.

The transverse circulations show small-scale oscillations that increase as internal mixing is increased. This paradox results from balancing "noise" in the prescribed tangential wind profiles by oscillations in the radial and vertical advection terms.

1. INTRODUCTION

The tangential wind distribution for mature hurricanes is relatively well known from aircraft measurements. Several investigators (Krishnamurti 1961, 1962; Barrientos 1964) have calculated the transverse or meridional circulations required to maintain specified (observed) tangential wind distributions in a steady state with various assumptions concerning horizontal and vertical mixing. Krishnamurti (1961, 1962) used the method of characteristics in both axisymmetric and asymmetric models. Barrientos (1964) extended Krishnamurti's work on the axisymmetric model by adding a more realistic boundary layer.

Both Barrientos and Krishnamurti considered relatively small domains (less than 200 km from the center of the storm). In this paper, transverse circulations are obtained for a prescribed tangential wind distribution over a domain extending 1000 km from the center. An iterative method is used to compute the steady-state vertical velocity at the top of the boundry layer. This method gives more satisfactory solutions than the approximate formula used by Barrientos, especially in regions of small absolute vorticity.

The transverse circulations are quite reasonable inside 300 km. However, vertical circulations at larger distances require unreasonable amounts of diabatic heating and cooling to maintain the steady state. This difficulty is related to the angular momentum budget in the steady axisymmetric hurricane and can be eliminated if the symmetry assumption is relaxed.

The present calculations are carried out in isentropic coordinates to emphasize the relation between heating and angular momentum. In retrospect, however, this advantage is offset by the increased complexity of the continuity equation.

2. BASIC EQUATIONS

The steady-state equations of motion in cylindrical isentropic coordinates are

$$v_r\frac{\partial v_r}{\partial r}+\frac{d\theta}{dt}\frac{\partial v_r}{\partial\theta}+\frac{v_\lambda}{r}\frac{\partial v_r}{\partial\lambda}-fv_\lambda-\frac{v_\lambda^2}{r}=-\frac{\partial\psi}{\partial r}+F_r \tag{1}$$

and

$$v_r\zeta_a+\frac{d\theta}{dt}\frac{\partial v_\lambda}{\partial\theta}+\frac{v_\lambda}{r}\frac{\partial v_\lambda}{\partial\lambda}=-\frac{1}{r}\frac{\partial\psi}{\partial\lambda}+F_\lambda \tag{2}$$

where v_λ is the tangential velocity, positive in direction of increasing λ; v_r is the radial velocity; $d\theta/dt$ (the rate of potential temperature change following a parcel) is the "vertical velocity" in isentropic (θ) coordinates due to diabatic heating; f is the Coriolis parameter (5.0×10^{-5} $\sec^{-1}$); and F_r and F_λ are expressions for the mixing of radial and tangential momentum, respectively. The mixing expressions are written in terms of constant horizontal (K_H) and vertical (K_Z) mixing coefficients:

$$F_\lambda=K_H\left(\frac{\partial^2 v_\lambda}{\partial r^2}+\frac{1}{r}\frac{\partial v_\lambda}{\partial r}-\frac{v_\lambda}{r^2}\right)+K_Z\frac{\partial^2 v_\lambda}{\partial Z^2} \tag{3}$$

with a similar expression for F_r. It is recognized that this Fickian type of mixing in numerical modeling is only a gross approximation to the role of turbulence in nature. Constant mixing coefficients seem to be particularly inadequate to represent vertical mixing in hurricanes, where the importance of cumulus clouds in the redistribution of momentum has been demonstrated by Gray (1967). In this paper, however, it is shown (section 7) that the inclusion of *any* form of internal mixing leads to unrealistic results, because the specified (observed) tangential winds are not free to vary with the amount or form of mixing.

The Montgomery potential, ψ, and the absolute vorticity, ζ_a, are defined by

$$\psi=c_pT+gz \tag{4}$$

and

$$\zeta_a=\frac{\partial rv_\lambda}{r\partial r}+f \tag{5}$$

where c_p is the specific heat at constant pressure, T is absolute temperature, g is the acceleration of gravity, and z is height.

The hydrostatic equation is

$$\frac{\partial\psi}{\partial\theta}=c_p\frac{T}{\theta}, \tag{6}$$

and the definition of potential temperature is

$$\theta=T\left(\frac{P_0}{p}\right)^\kappa \tag{7}$$

where $P_0=1000$ mb, p is pressure, and $\kappa=0.287$.

The equations for the circularly averaged motion at distance r from the center are derived by letting

$$v_r\equiv\overline{v_r}+v_r'$$

and (8)

$$v_\lambda\equiv\overline{v_\lambda}+v_\lambda'$$

where

$$(\overline{\ \ })\equiv\frac{1}{2\pi}\int_0^{2\pi}(\ \ )d\lambda. \tag{9}$$

After substituting (8) into equations (1) and (2) and applying the operator defined by (9), the equations describing the mean motion are

$$\overline{v_r}\frac{\partial\overline{v_r}}{\partial r}+\overline{v_r'\frac{\partial v_r'}{\partial r}}+\overline{\frac{d\theta}{dt}\frac{\partial v_r}{\partial\theta}}-f\overline{v_\lambda}-\frac{\overline{v_\lambda}^2}{r}-\frac{\overline{v_\lambda'^2}}{r}=-\frac{\partial\overline{\psi}}{\partial r}+\overline{F_r} \tag{10}$$

and

$$\overline{v_r}\,\overline{\zeta_a}+\overline{v_r'\zeta_a'}+\overline{\frac{d\theta}{dt}\frac{\partial v_\lambda}{\partial\theta}}=\overline{F_\lambda}. \tag{11}$$

The averaged continuity equation in isentropic coordinates is

$$\frac{1}{r}\frac{\partial r\overline{v_r}}{\partial r}\frac{\partial p}{\partial\theta}+\frac{\partial}{\partial\theta}\overline{\frac{d\theta}{dt}\frac{\partial p}{\partial\theta}}=0 \tag{12}$$

where we have assumed that $\partial p/\partial\theta=\overline{\partial p}/\partial\theta$. Multiplying equation (11) by $\partial p/\partial\theta$, defining

$$U\equiv\overline{v_r}\frac{\partial p}{\partial\theta} \tag{13}$$

and

$$W\equiv\overline{\frac{d\theta}{dt}}\frac{\partial p}{\partial\theta}, \tag{14}$$

and eliminating U between equations (11) and (12), we obtain the following first-order differential equation in W:

$$\frac{\partial W}{\partial\theta}-d\frac{\partial W}{\partial r}-\frac{\partial rd}{r\partial r}W+E(r,\theta)-\frac{1}{r}\frac{\partial r\frac{\partial p}{\partial\theta}\overline{v_r'\zeta_a'}/\overline{\zeta_a}}{\partial r}=0. \tag{15}$$

In (15), $d\equiv(\partial v_\lambda/\partial\theta)/\overline{\zeta_a}$ and $E(r,\theta)\equiv(1/r)(\partial)(r\partial p/\partial\theta)(\overline{F_\lambda}/\overline{\zeta_a})/\partial r$. The expressions for d, $\partial rd/r\partial r$, and E may be calculated by finite differences from the prescribed tangential wind distribution, so that (15) is an equation in two unknowns, W and $\overline{v_r'\zeta_a'}$. In the axisymmetric case, $\overline{v_r'\zeta_a'}=0$, and (15) may be solved numerically for $W(r,\theta)$ given $W(r,\theta_0)$ and $W(r_0=0,\theta)$ as boundary conditions. Tne radial velocity may be calculated from (13) where

$$U=\left(\frac{\partial p}{\partial\theta}F_\lambda-W\frac{\partial v_\lambda}{\partial\theta}\right)/\overline{\zeta_a}. \tag{16}$$

The solution for $\overline{v_r'\zeta_a'}=0$ corresponds to the axisymmetric results of Krishnamurti (1961) and Barrientos (1964). We show that the solutions from this form of the equation are reasonable near the center of the hurricane, but unreasonable at larger distances. The unreasonable solutions for $d\theta/dt$ at larger distances apparently result from either the steady-state assumption or the neglect of $\overline{v_r'\zeta_a'}$ in (15). We investigate the latter possibility by specifying $d\theta/dt$ beyond some distance from the storm center and calculating $\overline{v_r'\zeta_a'}$. The pattern and order of magnitude of this mean eddy term is then compared with empirical evidence.

3. STRUCTURE OF THE MODEL

The geometry of the model consists of the sea level surface and 14 isentropic surfaces (305° to 370°K). The velocity components v_λ and v_r, $d\theta/dt$, and $\partial p/\partial\theta$ are defined at even θ surfaces. The other variables are defined at odd θ surfaces. Given $T(\theta)$ at $R=1000$ km from Jordan's (1958) mean hurricane season sounding, $\psi(\theta)$ at $R=1000$ km is computed from the hydrostatic equation. An estimate on the temperature distribution is computed by integrating the gradient wind equation

$$\frac{\partial\psi}{\partial r}=fv_\lambda+\frac{v_\lambda^2}{r} \tag{17}$$

from $r=1000$ km to $r=0$ to obtain $\psi(\theta)$ and then differentiating $\psi(\theta)$ to calculate T. Note that the gradient wind assumption is used only to obtain an *estimate* of the temperature structure, and the vortex circulation is not assumed to be in gradient balance in the other calculations.

The surface pressure is determined by assuming that the pressure gradient at the surface equals the pressure gradient at $\theta=310$°K. We also assume $T(z=0)=27$°C, which defines $\theta(z=0)$ by equation 7. Because the variables are calculated at alternate θ levels, values for the intermediate levels are linearly interpolated as needed.

Equation (15) may be solved as a mixed initial value and boundary value problem. To calculate $W(\theta_0, r)$, we make use of the steady-state thermodynamic equation in pressure coordinates:

$$\frac{d\theta}{dt}=\omega\frac{\partial\theta}{\partial p}+v_r\frac{\partial\theta}{\partial r}. \tag{18}$$

Since the major inflow occurs in the boundry layer, $v_r(\partial\theta/\partial r)$ may be neglected in comparison to $\omega(\partial\theta/\partial p)$ at the top of the boundary layer. The steady-state ω at the top of the boundary layer (ω_T) is calculated by an iterative technique described in the next section. We then approximate $W(r, \theta=305) \approx (d\theta/dt)(\partial p/\partial\theta)$.

At the origin, (15) reduces to

$$\frac{\partial W}{\partial\theta} = -E(r=0, \theta) \tag{19}$$

by the symmetry assumption. The solution to equation (19) is

$$W(r=0, \theta) = W(r=0, \theta=305) e^{-\int_{\theta_0}^{\theta} E(r=0,\theta)\,d\theta} \tag{20}$$

Equation (20) is solved numerically to yield $W(r=0, \theta)$, the other necessary boundary condition.

4. THE VERTICAL VELOCITY AT THE TOP OF THE BOUNDARY LAYER

To calculate the steady-state ω_T for the pressure gradient force, $F(r)$, we assume a boundary layer of fixed depth, $\Delta p = 100$ mb. The tangential and radial equations of motion are written for the middle level in the boundary layer, where we assume that the horizontal advection of momentum dominates the vertical advection:

$$\frac{\partial rv_\lambda}{\partial t} = -v_r \frac{\partial rv_\lambda}{\partial r} - frv_r + r\left\{\frac{-C_D g\rho|\mathbf{V}|}{\Delta P} v_\lambda + \frac{1}{r^2}\frac{\partial}{\partial r} K_H r^3 \frac{\partial v_\lambda/r}{\partial r}\right\} \tag{21}$$

and

$$\frac{\partial v_r}{\partial t} = -v_r \frac{\partial v_r}{\partial r} + fv_\lambda + \frac{v_\lambda^2}{r} - F(r) \frac{-C_D g\rho|\mathbf{V}|}{\Delta P} v_r + \frac{1}{r^2}\frac{\partial K_H}{\partial r} r^3 \frac{\partial v_r/r}{\partial r}. \tag{22}$$

In (21) and (22), C_D is the drag coefficient, ρ is the surface density, and $|\mathbf{V}| = (v_\lambda^2 + v_r^2)^{1/2}$. The nonlinear horizontal mixing is modeled after Smagorinsky (1965). For cylindrical coordinates and circular symmetry,

$$K_H = k_0^2 (\Delta r)^2 |D| \tag{23}$$

where

$$|D| = r\left\{\left[\frac{\partial v_r/r}{\partial r}\right]^2 + \left[\frac{\partial v_\lambda/r}{\partial r}\right]^2\right\}^{1/2}. \tag{24}$$

In equation (23), k_0 is a nondimensional constant of order unity.

The steady-state radial and tangential velocities that correspond to the pressure gradient force, $F(r)$, are computed iteratively using the Matsuno (1966) differencing scheme. This scheme has the desirable property of damping high-frequency waves. One iteration cycle is summarized below, with the superscript referring to the iteration step:

1) Given values of v_λ^n and v_r^n, "forecast" tentative values (designated by v_λ^* and v_r^*) of v_λ^{n+1} and v_r^{n+1} from equations (21) and (22).

2) "Forecast" final estimates of v_λ^{n+1} and v_r^{n+1} using * values of v_λ and v_r where they appear in the right sides of (21) and (22).

3) Return to 1.

This completes one iteration cycle. The iterations continue until the root-mean square of the differences between successive iterations reaches some small value. After the steady radial velocities are attained, ω_T is computed from the continuity equation

$$\frac{\omega_T - \omega_0}{\Delta P} = \frac{(rv_r)_{j+1} - (rv_r)_j}{r_{j+\frac{1}{2}}\Delta r} \tag{25}$$

with $\omega_0 = 0$. The index j refers to the horizontal grid point with $r_j = (j-1)\Delta r$.

Centered differences are used for the advective terms. Boundary conditions at 1000 km are zero divergence and zero relative vorticity. Other parameters are $k_0 = 0.5$, $C_D = 0.003$, $\rho = 1.0\times10^{-3}$ gm cm^{-3}, $\Delta r = 20$ km, and $\Delta t = 120$ sec.

The iterative method for computing the steady-state ω_T is quite powerful and has relatively few restrictions. In contrast, the approximate expression

$$\omega_T \approx \frac{-g}{r}\frac{\partial[rC_D\rho|\mathbf{V}|v_\lambda/\zeta_a]}{\partial r} \tag{26}$$

used by Anthes and Johnson (1968) and Barrientos (1964) yields unsatisfactory solutions for profiles with small values of absolute vorticity.

5. COMPUTATIONAL PROCEDURE

For the axisymmetric calculation in which $\overline{v_r'\zeta_a'}$ is assumed zero, (15) is solved in two ways. The first method is explicit and uses forward θ differencing and one-sided r differencing in computing $d(\partial W/\partial r)$. The finite-difference equation for (15) is

$$W_j^{n+1} = \left[1 - \frac{\Delta\theta}{\Delta r}|d_j^n| + \Delta\theta\left(\frac{\partial rd}{r\partial r}\right)_j^n\right] W_j^n + \frac{\Delta\theta}{\Delta r}|d_j^n| W_{j+1}^n - \Delta\theta E_j^n. \tag{27}$$

In equation (27), $\Delta\theta$ is the increment of θ, and n refers to the θ level. In all experiments $\Delta r = 20$ km. The size of $\Delta\theta$ depends on the computational stability requirement $|(\Delta\theta/\Delta r)d| < 1$. To satisfy this requirement, $\Delta\theta$ varies from 1°K in the low levels to 0.125°K in the upper levels. The term $(\partial rd/r\partial r)_j^n$ is approximated by $(r_{j+1}d_{j+1}^n - r_{j-1}^n d_{j-1})/r_j(r_{j+1} - r_{j-1})$.

The advantage in this first method is that $d = (\partial v_\lambda/\partial\theta)/\zeta_a$ may be either positive or negative. In the implicit method discussed later, d must be negative, which restricts

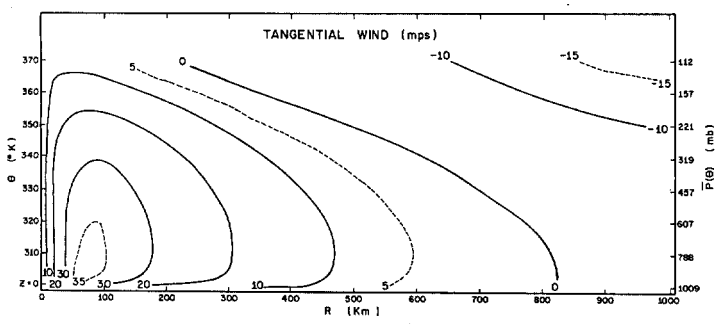

FIGURE 1.—Specified tangential wind distribution used in computing transverse circulations for all experiments.

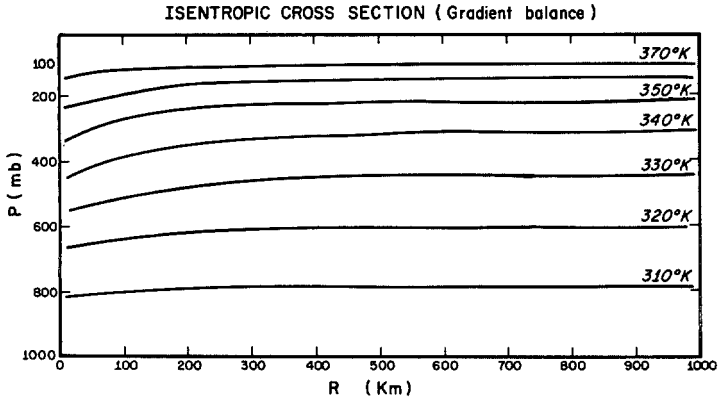

FIGURE 2.—Isentropic cross section computed from tangential wind distribution shown in figure 1 assuming gradient balance.

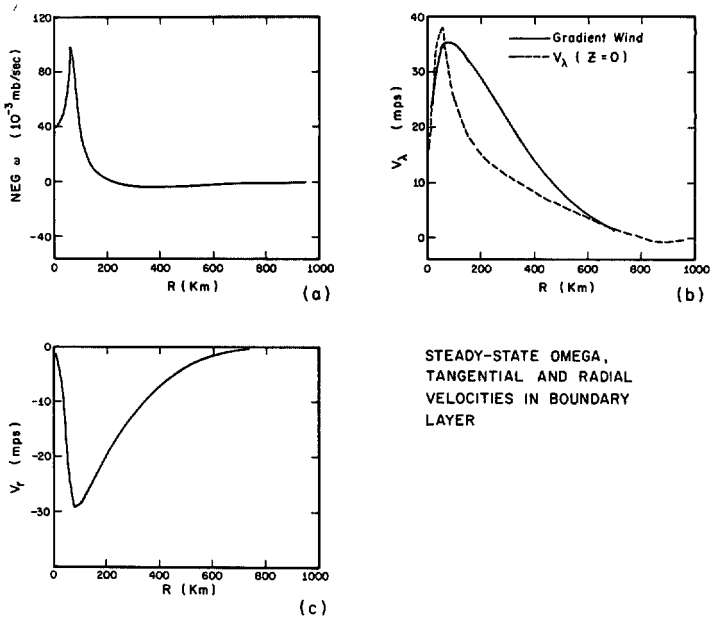

STEADY-STATE OMEGA, TANGENTIAL AND RADIAL VELOCITIES IN BOUNDARY LAYER

FIGURE 3.—(a) steady-state vertical motion profile at the top of the boundary layer computed iteratively under a steady pressure gradient force; (b) gradient tangential wind (solid line) at the top of the boundary layer and steady-state tangential wind (dashed line) at the middle level in the boundary layer; and (c) steady-state radial velocity at the middle level in the boundary layer.

this method to regions where the cyclonic winds decrease with height. The chief disadvantage of the first method is that very small $\Delta\theta$ steps are required in the upper levels where $|(\partial v_\lambda/\partial\theta)/\zeta_a|$ is large.

An implicit finite-difference scheme has the advantage of computational stability for any $\Delta\theta$ and Δr provided that $d < 0$ everywhere. The implicit finite-difference equation corresponding to (15) is

$$W_j^{n+1}=\left\{\left[1+\frac{\Delta\theta}{2\Delta r}\overline{d}_j^{\theta}+\frac{\Delta\theta}{2}\frac{\overline{\partial r d}^{\theta}}{r\partial r_j}\right]W_j^n-\frac{\Delta\theta}{2\Delta r}\overline{d}_j^{\theta}W_{j-1}^n\right.$$

$$\left.-\frac{\Delta\theta}{2\Delta r}\overline{d}_j^{\theta}W_{j-1}^{n+1}-\Delta\theta\overline{E}_j^{\theta}\right\}\div\left[1-\frac{\Delta\theta}{2\Delta r}\overline{d}_j^{\theta}-\frac{\Delta\theta}{2}\frac{\overline{\partial r d}^{\theta}}{r\partial r_j}\right] \quad (28)$$

where

$$\overline{(\ )}^{\theta}=\tfrac{1}{2}[(\ )^{n+1}+(\ )^n].$$

In the experiments shown here, $d < 0$ everywhere so equation (28) is used in most of the experiments. In one comparison experiment, the maximum differences in results between the explicit and the implicit schemes were on the order of 3 percent.

6. RESULTS

The prescribed vertical cross section of tangential wind used in all the experiments is shown in figure 1. The isentropic cross section assuming gradient balance above the boundary layer is shown in figure 2. The steady-state tangential and radial winds in the boundary layer and the corresponding ω at the top of the boundary layer are shown in figures 3a through 3c.

A list of the experiments and their main characteristics are given in table 1.

Experiment 1 calculates the transverse circulations with no explicit mixing. Figure 4 shows Stokes's stream function, Φ, defined by

$$\frac{1}{r}\frac{\partial\Phi}{\partial r}=W$$

and (29)

$$\frac{1}{r}\frac{\partial\Phi}{\partial\theta}=-U.$$

The meridional circulation shows inflow in the boundary layer, rising motion inside 240 km, outflow in the middle and upper troposphere, and sinking motion at large distances from the center. The corresponding vertical motion and radial velocity cross sections are shown in figures 5 and 6. The approximate vertical motion is computed from

$$w\approx-\omega/\rho g. \quad (30)$$

Figure 4 shows the angular momentum ($M\equiv(fr^2/2)+rv_\lambda$) cross section. With no dissipation above the boundary layer, angular momentum should be conserved. Therefore, deviations between the streamlines and isolines of angular momentum are a measure of the truncation error in the finite-difference scheme. The streamlines cross toward

TABLE 1.—*List of experiments*

Exp. no.	K_H(cm² sec⁻¹)	K_Z(cm² sec⁻¹)
1	0.0	0
2	5.0×10^8	0
3	10.0×10^8	0
4	0.0	5×10^5

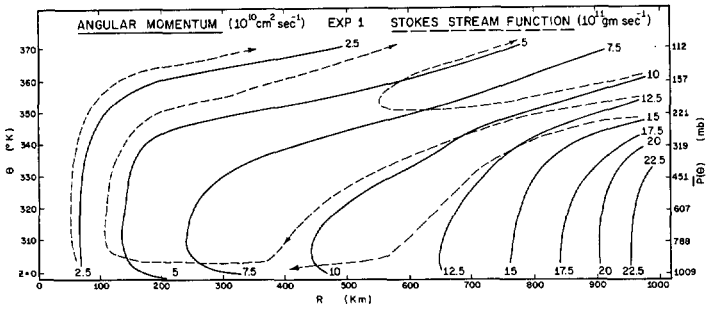

FIGURE 4.—Stokes's stream function (dashed lines) for experiment 1 with no horizontal or vertical mixing. Solid lines are angular momentum contours associated with assumed tangential wind distribution.

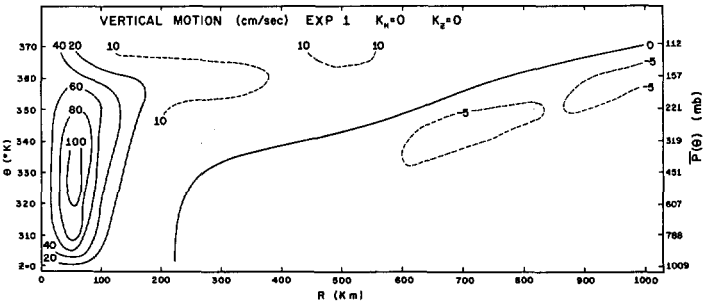

FIGURE 5.—Vertical motion cross section for experiment 1 (no horizontal or vertical mixing).

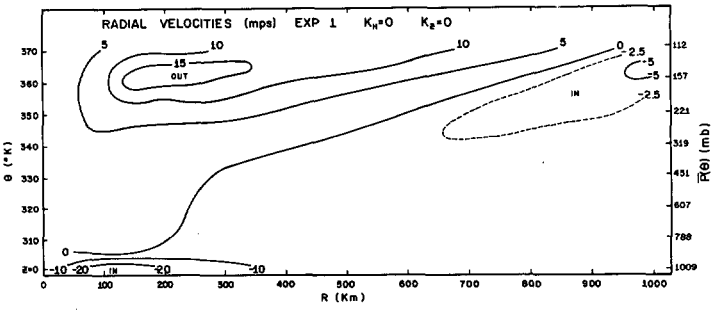

FIGURE 6.—Radial velocity cross section for experiment 1 (no horizontal or vertical mixing).

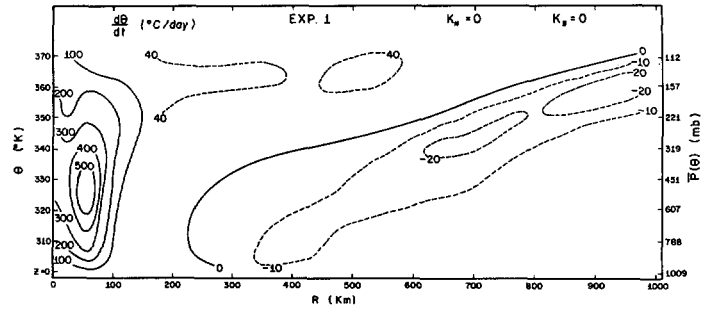

FIGURE 7.—Cross section of potential temperature change $d\theta/dt$ by diabatic heating required in steady-state experiment 1.

lower angular momentum, indicating that the truncation is dissipative. This is not surprising in view of the one-sided differencing in equation (28).

The difficulty with the computed circulations at large distances from the center is most apparent in the heating distribution. Figure 7 shows the cross section of $d\theta/dt$. The values near the center are fairly reasonable when the equivalent latent heating is converted to rainfall rates and compared with observations (table 2). At large distances from the center, however, temperature changes by diabatic heating are too large for the physical sources and sinks of energy at these distances. Heating near the tropopause is as much as 45°C day^{-1}, and cooling in the descending branch of the meridional circulation reaches 30°C day^{-1} in places. Since radiative effects are on the order of a few degrees per day, these solutions are considered unreasonable.

The difficulty arises from the axisymmetric assumption. Since $M=(fr^2/2)+rv_\lambda$, the isolines of mean angular momentum intersect the horizontal isentropic surfaces at greater angles with increasing r. With the symmetry assumption, this increasing angle of intersection implies large amounts of heating and cooling because angular momentum is approximately conserved. Friction causes the streamlines in the outflow layer to deviate toward lower values of angular momentum and requires even more diabatic heating.

Although Riehl and Malkus (1961) have shown that the asymmetries are unimportant inside 200 km, various investigators (Palmén and Riehl 1957, Pfeffer 1958) have found large contributions to the angular momentum budget from large-scale horizontal eddies at greater distances from the storm center. If these asymmetries oppose the mean flow in transporting angular momentum, the large diabatic heating shown by figure 7 would not be necessary to maintain the steady state. Because the mean outflow is directed toward higher values of angular momentum, the eddies must transport angular momentum inward .The converse is true for the mean inflow above the boundary layer.

In the axisymmetric model, the role of eddies can be calculated only as a mean effect represented by $\overline{v_r'\zeta_a'}$ in equations (11) and (15). If the heating (or $d\theta/dt$) is specified beyond some radius R^*, the mean radial velocity may be calculated for $r > R^*$ from (12), and $\overline{v_r'\zeta_a'}$ from (11). Figure 8 shows $\overline{v_r'\zeta_a'}$ for $R^*=400$ km in experiment 1, assuming $d\theta/dt=0$ beyond 400 km. The negative values in the upper troposphere show that the radial velocity and absolute vorticity must be negatively correlated. In the low levels, the correlation must be positive to balance

TABLE 2.—*Rainfall rates*

Radial ring	Experiment number			
	1	2	3	4
(*km*)		(*cm day*$^{-1}$)		
0–100	74.1	81.1	88.1	82.2
100–200	14.2	15.7	17.2	16.7
200–300	2.0	2.3	2.8	3.6
300–400	1.3	1.8	2.5	2.2
400–500	1.0	1.2	1.7	1.6

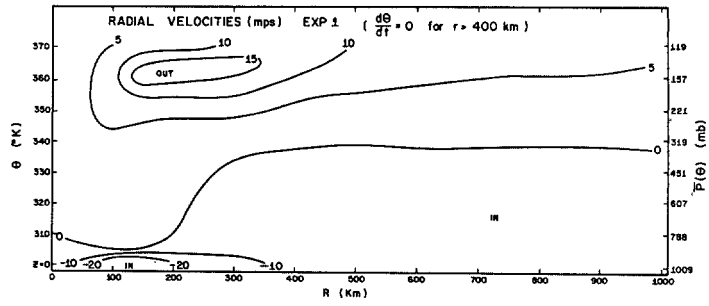

FIGURE 9.—Mean radial velocity (v_r) cross section for experiment 1 with no diabatic heating beyond 400 km.

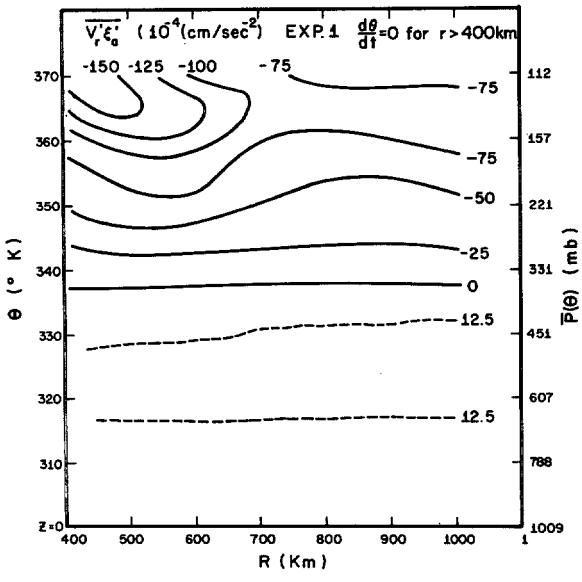

FIGURE 8.—Cross section of correlation between radial velocity (v_r) and absolute vorticity (ζ_a) required to balance mean transverse circulation by horizontal eddies for no diabatic heating beyond 400 km.

the mean flow, although the required magnitude is less than that in the outflow layer.

Clearly, the numerical values and the distribution of $\overline{v_r'\zeta_a'}$ depend strongly on the radius, R^*. Choice of R^* equal to 400 km in this case is based on the reasoning that the zero heating should begin near the radius where the boundary layer vertical motion becomes negative and the primary source of moisture is removed. Furthermore, unrealistic heating and cooling rates result for larger R^*. Computations with R^* equal to 600 and 800 km show the same sign distribution of $\overline{v_r'\zeta_a'}$, but slightly smaller values as R^* increases.

Qualitative evidence for the negative correlation between upper level outflow and absolute vorticity is present in synoptic cases that show strong outflow to occur anticyclonically in one quadrant of the storm. See, for example, the asymmetric outflow associated with the 1969 hurricane Camille (Parmenter 1969). Quantitative evidence requires computing $\overline{v_r'\zeta_a'}$ for individual storms. Unfortunately, the region of 400–1000 km is a region of relatively sparse hurricane data, as hurricane reconnaissance planes usually concentrate on obtaining data for the interior of the storm. However, support for the present hypothesis is found in the data of Izawa (1964), who computed mean wind structure from 14 typhoons. Izawa presents horizontal mean cross sections of v_r and ζ for 10 levels. A rough calculation from Izawa's data at 12 km (about 200 mb) shows values for $\overline{v_r'\zeta_a'}$ of -25 and -99×10^{-4} cm sec^{-2} for radii of 500 and 400 km, respectively. These values, which are of the same sign and nearly the same magnitude as the values shown in figure 8, support the hypothesis that large-scale asymmetries are important in the angular momentum budget at large distances from the hurricane center. Because these values are computed from mean data in which many of the individual asymmetries have been eliminated by the averaging process, it is likely that larger magnitudes are present in particular storms.

Figure 9 shows the corresponding radial velocities with no heating beyond 400 km. In contrast to the case with heating (fig. 6), the depth of the inflow and outflow layers remains constant with increasing r.

7. HORIZONTAL AND VERTICAL MIXING

Experiments 2, 3, and 4 investigate the effect of horizontal and vertical mixing on the transverse circulations. The results are quite ambiguous, however, because the tangential winds are forced to remain constant as the mixing is varied. In this type of model, small-scale variations in the tangential wind profiles remain in spite of any amount of mixing. The compensating radial advection required to maintain this "noise" produces oscillations in the radial motion profiles. The greater the mixing, the greater the oscillations must become, which is physically unreasonable since increased mixing should produce smoother profiles. This property is a fundamental defect in this type of model, rather than a computational problem.

Figures 10 and 11 show the radial wind and $d\theta/dt$ cross sections for experiment 2 in which $K_H=5\times10^8$ cm^2 sec^{-1} and $K_Z=0$. The overall effect of increasing the

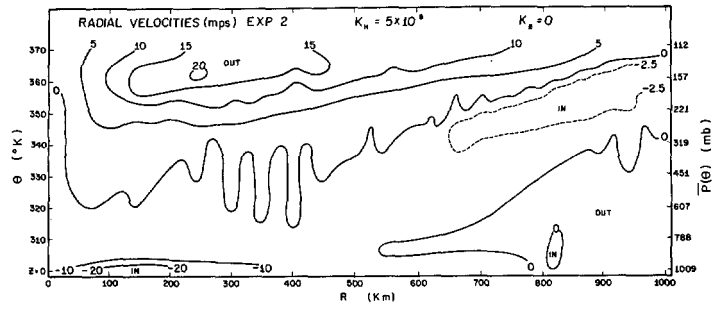

FIGURE 10.—Mean radial velocity cross section for experiment 2 (horizontal mixing with no vertical mixing).

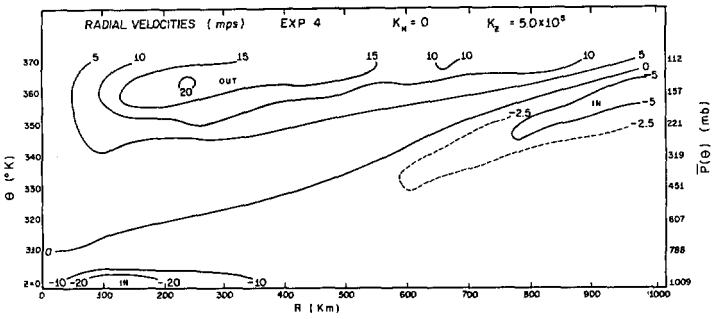

FIGURE 12.—Mean radial velocity cross section for experiment 4 (vertical mixing with no horizontal mixing).

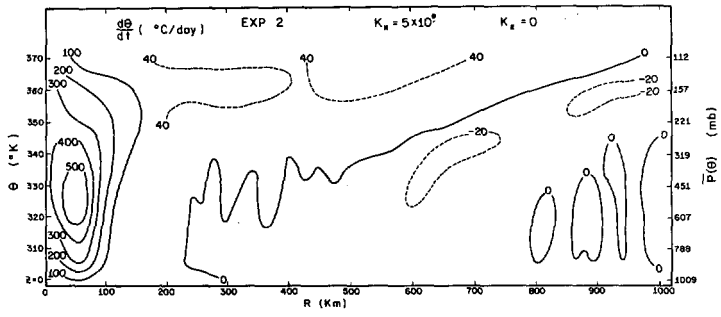

FIGURE 11.—Cross section of potential temperature change ($d\theta/dt$) by diabatic heating in experiment 2 (horizontal mixing with no vertical mixing).

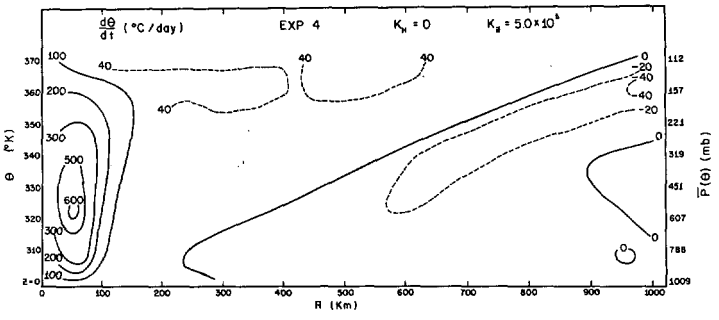

FIGURE 13.—Cross section of potential temperature change ($d\theta/dt$) by diabatic heating in experiment 4 (vertical mixing with no horizontal mixing).

horizontal mixing is to increase the upward motion and the outflow while decreasing the sinking motion, as additional angular momentum loss causes the streamlines to deviate toward lower values of angular momentum.

The increased noise in the v_r and $d\theta/dt$ fields is evident in both figures 10 and 11. Since tangential wind profiles taken from observations (for example, aircraft data) may be expected to have more noise than the profiles used here, an objective smoothing or filtering technique will be required to obtain reasonable solutions.

In experiment 3, the horizontal mixing coefficient K_H is increased to 10×10^8 cm^2 sec^{-1}. As expected, the amplitude of the v_r and $d\theta/dt$ oscillations increase over those found in experiment 2. The figures are not produced here.

While noise in the radial profiles of tangential wind produces vertically oriented eddies, noise in the vertical profiles of v_λ produce horizontally oriented eddies. Figures 12 and 13 show the radial velocities and $d\theta/dt$ for experiment 4 in which $K_H = 0$ and $K_Z = 5 \times 10^5$ cm^2 sec^{-1}. The additional source of cyclonic momentum in the upper levels by the vertical mixing term requires stronger outflow to balance the observed tangential winds. For example, the maximum outflow at 900 km increases from 4 m sec^{-1} in experiment 1 to 12 m sec^{-1} in experiment 4.

Apparently the "noise" in the vertical profile of v_λ is less than that in the horizontal profiles, since the oscillations in figures 12 and 13 are less pronounced than those in figures 10 and 11. This is probably a consequence of specifying the tangential wind at 51 points in the horizontal and only six points in the vertical.

TABLE 3.—*Diabatic heating and cooling*

Experiment no.	Heating	Cooling
	(10^{14} w)	(10^{14} w)
1	15.7	−10.8
2	18.8	−10.4
3	22.6	−10.7
4	20.5	−13.0

The total heating budget for experiments 1–4 is summarized in table 3. All components are larger than empirical values by a factor of about 2 (Anthes and Johnson 1968). This is related to the large vortex chosen for this study. The increased intensity of the meridional circulation for increased internal mixing is indicated in table 3. The total heating ranges from 15.7×10^{14} watts (w) for no explicit mixing to 22.6×10^{14} w for experiment 3 in which $K_H = 10 \times 10^8$ cm^2 sec^{-1}. Since lateral mixing affects the meridional circulation mainly near the center, the cooling remains relatively constant as K_H is varied. The increased vertical mixing, on the other hand, requires additional cooling.

8. SUMMARY

Mean meridional circulations associated with a specified, steady tangential wind are calculated for a domain 1000 km in radial extent. While realistic solutions are obtained near the center, the vertical motions at larger distances require unreasonable amounts of diabatic heating and cooling to maintain a steady state in the axisymmetric case. It is shown that asymmetries (large-scale horizontal eddies) beyond 400 km could produce the required balance without requiring physically unreasonable heating rates. The mass and angular momentum budgets require negative correlation between radial velocities and absolute vorticity in the upper levels and positive correlation in the lower levels.

The results of several experiments show that this type of model, in which the tangential motion is prescribed, is unsuitable for investigating the role of internal mixing in hurricanes. The steady-state assumption forces small-scale "noise" in the tangential wind structure to be balanced by noise in the radial and vertical motions.

ACKNOWLEDGMENTS

The author wishes to thank Drs. Donald R. Johnson and Stanley L. Rosenthal for their helpful discussions during the course of this study.

REFERENCES

Anthes, Richard A., and Johnson, Donald R., "Generation of Available Potential Energy in Hurricane Hilda (1964)," *Monthly Weather Review*, Vol. 96, No. 5, May **1968**, pp. 291–302.

Barrientos, Celso S., "Computations of Transverse Circulation in a Steady State, Symmetric Hurricane," *Journal of Applied Meteorology*, Vol. 3, No. 6, Dec. **1964**, pp. 685–692.

Gray, William M., "The Mutual Variation of Wind, Shear, and Baroclinicity in the Cumulus Convective Atmosphere of the Hurricane," *Monthly Weather Review*, Vol. 95, No. 2, Feb. **1967**, pp. 55–73.

Izawa, Tatsuo, "On the Mean Wind Structure of Typhoon," *Technical Note* No. 2, Typhoon Research Laboratory, Meteorological Research Institute, Tokyo, Japan, Mar. **1964**, 19 pp.

Jordan, Charles L., "Mean Soundings for the West Indies Area," *Journal of Meteorology*, Vol. 15, No. 1, Feb. **1958**, pp. 91–97.

Krishnamurti, T. N., "On the Vertical Velocity Field in a Steady, Symmetric Hurricane," *Tellus*, Vol. 13, No. 2, May **1961**, pp. 171–180.

Krishnamurti, T. N., "Some Numerical Calculations of the Vertical Velocity Field in Hurricanes," *Tellus*, Vol. 14, No. 2, May **1962**, pp. 195–211.

Matsuno, Taroh, "Numerical Integrations of the Primitive Equations by a Simulated Backward Difference Method," *Journal of Meteorology*, Vol. 15, No. 1, Feb. **1966**, pp. 76–84.

Palmén, Erik H., and Riehl, Herbert, "Budget of Angular Momentum and Kinetic Energy in Tropical Cyclones," *Journal of Meteorology*, Vol. 14, No. 2, Mar. **1957**, pp. 150–159.

Parmenter, Frances C., "Picture of the Month—Hurricane Camille," *Monthly Weather Review*, Vol. 97, No. 11, Nov. **1969**, pp. 828–829.

Pfeffer, Richard L., "Concerning the Mechanics of Hurricanes," *Journal of Meteorology*, Vol. 15, No. 1, Feb. **1958**, pp. 113–119.

Riehl, Herbert, and Malkus, Joanne S., "Some Aspects of Hurricane Daisy, 1958," *Tellus*, Vol. 13, No. 2, May **1961**, pp. 181–213.

Smagorinsky, Joseph, Manabe, Syukuro, and Holloway, J. Leith, Jr., "Numerical Results From a Nine-Level General Circulation Model of the Atmosphere," *Monthly Weather Review*, Vol. 93, No. 12, Dec. **1965**, pp. 727–768.

[Received November 24, 1969; revised Feburary 24, 1970]